Swarming transitions of self-propelled particles with anisotropic social interactions

Zhanwei Gao [1,2,3,4,*] and Iain D. Couzin [1,3,4,†]
[1]Department of Collective Behaviour, Max Planck Institute of Animal Behavior, Konstanz, Germany
[2]School of Systems Science, Beijing Normal University, Beijing, China
[3]Centre for the Advanced Study of Collective Behaviour, University of Konstanz, Konstanz, Germany
[4]Department of Biology, University of Konstanz, Konstanz, Germany

(Received 29 April 2022; accepted 3 April 2025; published 13 May 2025)

Collective motion in living systems is observed across many scales, from bacterial colonies to insect swarms, fish schools, and bird flocks. In all cases the motility of individual cells or organisms both is influenced by and, in turn, influences the motion of others. While the mechanisms by which individuals sense and respond to others differ greatly among species, simplified models that capture general principles of social interactions, such as the Vicsek model, have proved insightful. Here we introduce anisotropic sensory perception (a feature common to many animal species) into the Vicsek model in order to evaluate how this feature impacts collective motion. We find that, when the anisotropy $\alpha > 0$, meaning individuals are more influenced by neighbors ahead of them than those behind them, as the anisotropy becomes stronger, the swarming transition changes from the weak first-order transition observed for populations with isotropic perception to a stronger (i.e., more abrupt) first-order transition. Moreover, the critical noise threshold to achieve ordered motion decreases if α increases from zero to positive values. By contrast, when the anisotropy $\alpha < 0$, indicating individuals pay more attention to rearward neighbors, as the anisotropy becomes stronger, the order-disorder transition remains first order (at the thermodynamic limit) but becomes increasingly weak (less abrupt), and the critical noise threshold required to reach ordered motion increases slightly. An even simpler front-back semicircle model and an anisotropic model with vectorial noise are employed to further validate the respective roles those ahead and behind play in the emergence of collective motion. Taken together, our results demonstrate that the contribution of neighboring individuals to the collective motion in such particle systems significantly depends on their relative position to the focal particle. Frontal neighbors primarily enhance the strength of the first-order transition, whereas rearward neighbors progressively weaken it.

DOI: 10.1103/PhysRevResearch.7.023144

I. INTRODUCTION

Collective motion [1] is a striking phenomenon that is widely observed in group-living organisms across scales, from bacterial colonies [2–4] to insect swarms [5,6], fish schools [7–10], bird flocks [11–16], troops of primates [17], and even human crowds [18]. In all cases sensory inputs are fundamental drivers of social information transmission [19,20]. Groups of gregarious organisms, as a whole, often display an impressive variety of fascinating and spectacular collective patterns, such as swarming, milling, and schooling or flocking, and transitions between such collective patterns can take place spontaneously and/or in different contexts [10]. Similar patterns can be reproduced by models that exhibit simple, local interactions [21,22]. In particular these systems often exhibit abrupt transitions between disordered motion and ordered collective motion, which can be reproduced by simple interaction models like the standard Vicsek model (SVM) [23]. The SVM, a minimal model of self-propelled particles, was initially thought to exhibit a continuous (second-order) phase transition. However, the nature of the phase transition was shown to be discontinuous (first-order), with the apparent continuity being due to strong finite-size effects [24–26]. Subsequent studies revealed a much richer and more complex picture of the nature of these phase transitions [25,26]. Bertin *et al.* [27] demonstrated that as the system nears the transition, the homogeneous flow becomes unstable under finite-wavelength perturbations, leading to a nontrivial spatiotemporal flow pattern. Ihle [28] showed that the shape of invasion waves, which play a critical role in discontinuous phase transitions at moderate system sizes, can be quantitatively predicted using an inhomogeneous mean-field kinetic theory. Moreover, Solon and Tailleur [29,30] introduced a paradigm shift by redefining the transition as a phase separation between a disordered gas and an ordered liquid, resulting in two distinct transitions rather than a single one. Most recently, Kürsten and Ihle [31] uncovered a new phase in the SVM: the polar-ordered cross-sea phase, characterized by

*Contact author: izhanweigao@gmail.com
†Contact author: icouzin@ab.mpg.de

crossing waves with an inherently selected crossing angle, further enriching our understanding of the system's phase behavior.

As noted above, in the SVM, each identical pointwise particle is assumed to pay equal attention to all neighbors within its interaction range. Although that is a highly instructive simplification, recent experimental studies showed that it is more typical of individuals to explicitly respond anisotropically to their neighbors. For example, the influence of those ahead can be greater than that of those behind [7,8,12,32]. Such anisotropic social influence has been observed in various species, such as those that predominantly use vision to coordinate collective motion, such as schools of fish [7,8,19,32,33], flocks of pigeons [12] and storks [15], and troops of primates [17].

While greater influence of those ahead may seem like conclusive evidence of anisotropic interaction strengths, we note that frontal individuals may be more influential under conditions of completely isotropic interactions simply because individuals are moving forward. It is also regularly observed that individuals with knowledge or information about the location of food resources or migration routes usually occupy frontal positions in the group and guide the movement dynamics and decision-making of the collective [34,35]. If an individual ahead turns sharply, those behind will approach it more closely, at least transiently, whereas those ahead of it would tend to leave it behind. Despite this effect, however, there is growing experimental evidence that individuals can be explicitly more strongly influenced by those ahead, which makes sense since frontal individuals are experiencing the local environment which those behind will soon encounter. One exception to this may be marching bands of locusts, in which rearward individuals appear to be more influential, likely due to their propensity to cannibalize those ahead [36–39].

Thus, anisotropic interactions may be ubiquitous and may prove crucial to collective decision-making, pattern formation, and the functional complexity of groups as a whole. For example, recent studies have shown that anisotropic sensory perception can shape large-scale self-organized pattern formations [40,41]. While it has been shown that anisotropic interactions could result in the onset of collective motion [42], it remains unclear how anisotropic interactions contribute to the onset and maintenance of collective motion in the presence of noise.

In this paper, we employ a minimal model of self-propelled particles, in the spirit of the SVM, with anisotropic social interactions (hereafter denoted the AVM) and investigate the impact it has on the onset of collective motion. When anisotropy $\alpha > 0$, individuals are more strongly influenced by the neighbors in front of them than those behind them. As the anisotropy becomes stronger, this effect becomes more pronounced (as illustrated in Fig. 1). When anisotropy $\alpha < 0$, we consider the opposite effect, with rearward individuals being more influential than those ahead. The collective behaviors of a front-semicircle Vicsek model (FrontVM) and a back-semicircle Vicsek model (BackVM) are also investigated to verify that the frontal neighbors of a focal individual contribute oppositely to the strength (i.e., abruptness) of the first-order phase transition compared with those behind.

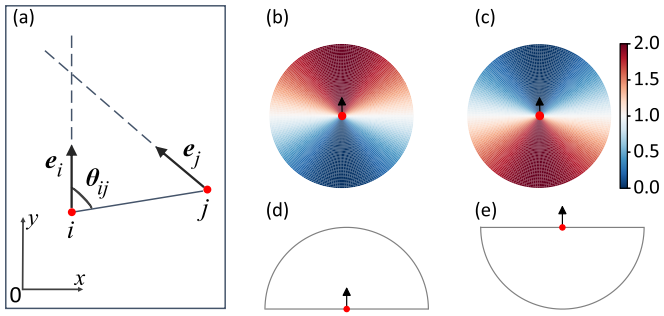

FIG. 1. Graphical representation of interactions between interacting particles. (a) Sketch of two interacting particles in the AVM, showing the moving orientations $\boldsymbol{e}_i$ and $\boldsymbol{e}_j$ of focal particle i and neighbor particle j, respectively. θ_{ij} is the angle between the angular position of particle j and the focal particle i. Two extreme cases of the AVM (b) for $\alpha = 1$ and (c) for $\alpha = -1$. (d) Front-semicircle Vicsek model. (e) Back-semicircle Vicsek model. Red dots and black arrows represent a particle and its moving orientation, respectively, for (a)–(e).

As in the SVM, initially, N identical pointwise particles, labeled by an integer index i, are randomly placed on a two-dimensional domain with size $L \times L$ with periodic boundary conditions. They move off lattice at constant speed v_0 at each discrete time step Δt by a fixed distance $v_0 \Delta t$ synchronously. Each particle i is defined by the orientation $\theta_i(t)$, the velocity $\boldsymbol{v}_i(t)$, constant speed $v_0 = |\boldsymbol{v}_i(t)|$, and the position $\boldsymbol{x}_i(t)$. The orientation of focal particle i is determined by the orientations of its neighbors (including itself) within the interaction radius $r = 1$. In the SVM, the orientation of particle i is updated at each time step $\Delta t = 1$ according to

$$\langle \theta_i(t) \rangle_r = \Theta \left[\sum_{d_{ij} < r}^{n_i} \boldsymbol{v}_j(t) \right], \tag{1}$$

where $\Theta[\boldsymbol{v}]$ denotes the angle of a vector $\boldsymbol{v}$ and n_i is the number of neighbors of particle i within the interaction radius r. In the AVM, instead of simply averaging equally over all neighbors as in the SVM, the influence of a neighbor particle j on the focal particle i is determined by the weight, $\Omega_{ij} = 1 + \alpha \cos(\theta_{ij})$ [22,43], where θ_{ij} is the angle between the moving orientation of focal particle i and the unit vector pointing from i to its neighbor j, as shown in Fig. 1, and $\alpha \in [-1, 1]$ is the anisotropy strength factor ($\alpha < 0$ means rearward neighbors are more influential). Thus, for the AVM, Eq. (1) can be rewritten as

$$\langle \theta_i(t) \rangle_r = \Theta \left[\boldsymbol{v}_i(t) + \sum_{d_{ij} < r, j \neq i}^{n_i - 1} \Omega_{ij} \boldsymbol{v}_j(t) \right]. \tag{2}$$

The orientation and position of particle i can then be updated according to

$$\theta_i(t + \Delta t) = \langle \theta_i(t) \rangle_r + \eta \xi_i(t), \tag{3}$$

$$\boldsymbol{x}_i(t + \Delta t) = \boldsymbol{x}_i(t) + \boldsymbol{v}_i(t + \Delta t) \Delta t, \tag{4}$$

respectively, where $\xi_i(t)$ is the angular noise, a random angle chosen from a uniform distribution within the interval $[-1/2, 1/2]$, and $\eta \in [0, 2\pi]$ is the noise strength.

The relative influence of neighbor particle j on focal particle i is determined by $\Omega_{ij} = 1 + \alpha\cos(\theta_{ij})$, and modulus $|\alpha|$ quantifies the strength of the anisotropy. With θ_{ij} increasing from 0 to π, the function $\cos(\theta_{ij})$ decreases monotonically from 1 to -1. Given any $j, k \in [1, N]$, $\theta_{ij} < \pi/2 < \theta_{ik}$ means particle j is a frontal neighbor of focal particle i, while particle k is a rearward neighbor. For $\alpha > 0$, $\Omega_{ij} > \Omega_{ik}$, which indicates focal particle i is more strongly influenced by frontal neighbor j. For $\alpha < 0$, $\Omega_{ij} < \Omega_{ik}$, indicating that focal particle i is more strongly influenced by rearward neighbor k. To highlight the general principle of the model, two extreme cases of the AVM are shown in Figs. 1(b) and 1(c) for $\alpha = 1$ and $\alpha = -1$, respectively. If $\alpha = 0$, our model is equivalent to the SVM. Note also that function $\cos(\theta_{ij})$ can be simply replaced by any complicated, but monotonic, function $f(i, j, \theta_{ij}) \in [-1, 1]$.

In the absence of noise ($\eta = 0$), all interacting particles align perfectly, while for maximal noise ($\eta = 2\pi$), particles follow random walks. With $\eta \in (0, 2\pi)$, the system varies between the two extreme limits. The transition between these two regimes can be conveniently characterized by the instantaneous order parameter (OP), $\varphi(t) \equiv \frac{1}{Nv_0}|\sum_{i=1}^{N} \boldsymbol{v}_i(t)|$, and its temporal average $\langle\varphi\rangle_t$. If the probability density function (PDF) of $\varphi(t)$ is unimodal, $\langle\varphi\rangle_t$ is averaged over all data, while if the PDF profile is bimodal, the data are divided into two parts by the valley point between the peaks and then averaged for the disordered and ordered states, respectively. The difference, or "gap," between the order parameters associated with the ordered and disordered phases (near the transition) has been used to characterize the strength of the first-order transition [44]. The so-called Binder cumulant $G(\eta, L) = 1 - \langle\varphi^4\rangle_t/(3\langle\varphi^2\rangle_t^2)$, proposed by Binder [45], is widely used to monitor the jump of $\langle\varphi\rangle_t$ [25,26,44]. In two dimensions, $G \approx 2/3$ in the ordered phase, and $G \approx 1/3$ in the disordered phase with unimodal Gaussian distributions of $\varphi(t)$. The Binder cumulant exhibits a sharp drop toward a minimum, smaller than 1/3, due to the simultaneous contributions of the phase coexistence in first-order phase transition, and if the drop in the Binder cumulant deepens enough to negative values, a strong first-order phase transition is then observed near the transition point η_c, at which disordered and ordered phases compete evenly at the thermodynamic limit due to bimodal distributions of $\varphi(t)$ [45]. So $\langle\varphi\rangle_t$ and G are used to characterize the nature of the phase transition. Additionally, the variance of $\varphi(t)$ is used to provide further evidence of a first-order transition if it is sharply peaked with a high value, and the higher the value is, the stronger the signal of the first-order phase transition is for such nonequilibrium systems. A more detailed discussion is provided in the Appendix.

II. RESULTS

By varying the anisotropy coefficient α, we find that the particle system exhibits a rich spectrum of phase transitions as a function of noise intensity η. Particularly, for $\alpha = 0$, where each particle exhibits isotropic social interactions and thus is influenced equally by all neighbors within the interaction

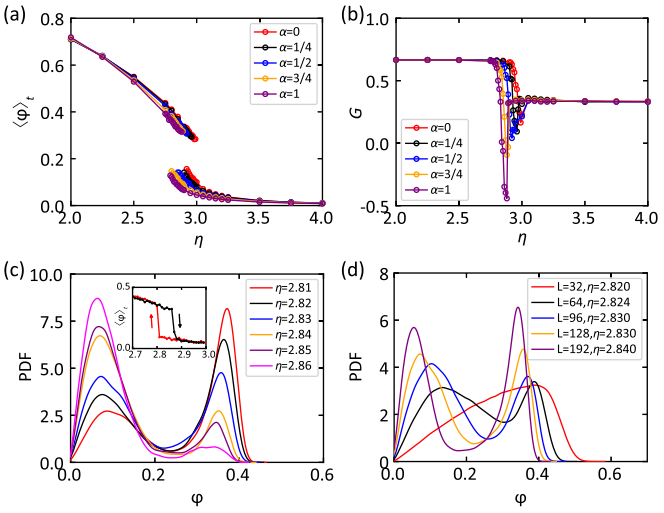

FIG. 2. Phase transitions of the AVM for $\alpha \geqslant 0$. (a) The time-averaged order parameter (collective alignment) $\langle\varphi\rangle_t$ as a function of noise amplitude η. (b) Binder cumulant G as a function of noise amplitude η, with the same symbols and colors as in (a). Time averages are computed over 1×10^6 time steps. (c) PDF of φ near the transition point with $\alpha = 1$. The hysteresis in the inset is shown at a fixed ramp rate of $1/2 \times 10^{-6}$ per time step (each data point is averaged over 2×10^4). Black solid circles indicate the path of adiabatic noise amplitude increase, while red solid circles represent the path of adiabatic decrease. (d) The finite-size effect near the transition point with $\alpha = 1$. The parameters are $\rho = 2$, $v_0 = 0.5$, and $L = 128$ for (a)–(c).

range, i.e., the SVM, a weak first-order phase transition is observed, but the gap (i.e., the difference in collective order) between the two phases near η_c is small, as is the decrease in G, as shown in Figs. 2(a) and 2(b).

For $\alpha > 0$, as α increases, corresponding to an increasing relative influence of frontal individuals, we find that while the critical noise at which the system transitions from disorder to order decreases, the gap becomes larger, and the minimum of G becomes deeper, characteristic of a stronger (more pronounced) first-order phase transition. When $\alpha = 1$, the enhanced discontinuity is maximal, as shown in Figs. 2(a) and 2(b). Figure 2(c) shows the bimodal PDFs of $\varphi(t)$ near the transition point η_c with $\alpha = 1$. The peak at larger values of $\varphi(t)$ and the other peak at smaller values correspond to the ordered phase and the disordered phase, respectively. As noise intensity increases, the ordered phase shrinks, and the disordered phase expands. Another classical hallmark of first-order phase transitions is the presence near the transition point of the hysteresis phenomenon. As clearly shown in Fig. 2(c), the hysteresis is formed by ramping the control parameter up and down at a fixed rate. For a system with fixed particle density $\rho = \frac{N}{L\times L}$, increasing the number of particles in the system is equivalent to increasing the system's size. Since the transitional properties also depend on the number of particles N, the finite-size effect analysis is shown in Fig. 2(d). As the system gets larger, the bimodal peaks become increasingly sharp, as is expected for systems exhibiting stronger first-order phase transitions. (Further detailed analysis is provided in the Appendix.)

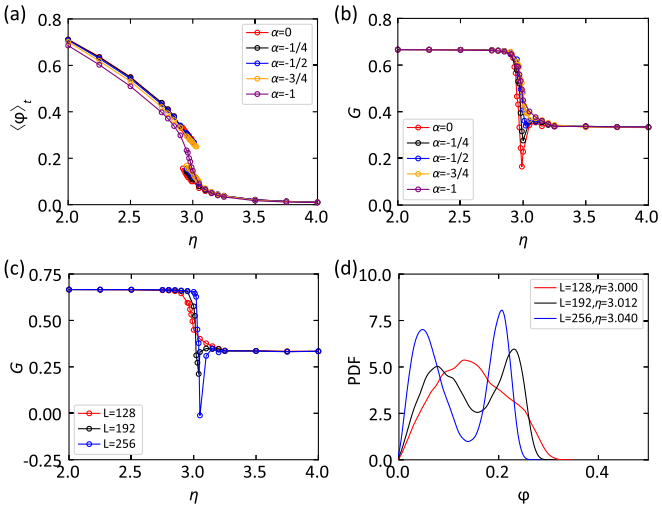

FIG. 3. Phase transitions of the AVM with $\alpha \leqslant 0$. (a) The time-averaged OP $\langle\varphi\rangle_t$ as a function of noise amplitude η. (b) Binder cumulant G as a function of noise amplitude η, with the same symbols and colors as in (a). (c) Binder cumulant G as a function of noise amplitude for various system sizes L with $\alpha = -1$. (d) The finite-size effect near the transition point with $\alpha = -1$. Time averages are computed over 1×10^6 time steps. The parameters are $\rho = 2$, $v_0 = 0.5$, and $L = 128$ for (a)–(c).

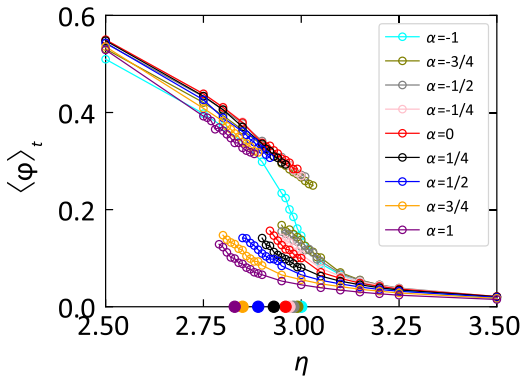

FIG. 4. Phase transitions of the AVM with $\alpha \in [-1, 1]$. The time-averaged OP $\langle\varphi\rangle_t$ as a function of noise amplitude η, with the corresponding transition point marked by a solid dot of the same color. Time averages are computed over 1×10^6 time steps. The parameters are $\rho = 2$, $v_0 = 0.5$, and $L = 128$.

We next consider the collective dynamics for $\alpha < 0$, where each particle with anisotropic interactions is more strongly influenced by rearward individuals. As α decreases, we find that while the critical noise does not change much, the gap becomes smaller, and the minimum of G gets shallower. When $\alpha = -1$, the curve of $\langle\varphi\rangle_t$ as a function of the noise amplitude η, becomes continuouslike, and the Binder cumulant G changes monotonically, with a minimum at $G \approx 1/3$ suggesting a continuouslike phase transition, as shown in Figs. 3(a) and 3(b). Further finite-size effect analysis, however, demonstrates that the nature of transitions for $\alpha = -1$ is still first order, as shown in Figs. 3(c) and 3(d). As the system gets larger, the minimum of G decreases to negative values, the PDF of $\varphi(t)$ changes from unimodal to bimodal, and the bimodal peaks become increasingly sharp, all indicative of first-order phase transitions.

As shown in Figs. 2(a) and 3(a), the critical noise threshold required to achieve ordered motion decreases as α increases from zero to positive values. In contrast, while the threshold increases as α decreases from zero to negative values, the change is less pronounced. To better highlight this effect, we combine both Figs. 2(a) and 3(a) into a single plot, as presented in Fig. 4. The transition points are marked by solid dots of the respective color, clearly illustrating the transition points.

A typical feature of the SVM is the formation of localized, high-density, and high-order traveling bands led by density fluctuations. The ordered traveling bands appear and dissolve over time near the transition point η_c. To better understand how anisotropic social response to near neighbors impacts the swarming transitions from order to disorder, we examine how the spatial distribution of the moving particles is affected. Four representative snapshots of the traveling flocks are shown in Figs. 5(a)–5(d), corresponding to the following cases: disordered isotropic ($\alpha = 0$), ordered isotropic ($\alpha = 0$), ordered positive anisotropic ($\alpha = 1$), and ordered negative anisotropic ($\alpha = -1$), respectively. The value of the global OP for all selected ordered cases $\varphi(t) \approx 0.36$, which allows for a clear comparison of the moving-band formations under different conditions. Figures 5(a) and 5(b) show the disordered case and the ordered case of the SVM (i.e., $\alpha = 0$), respectively. In the ordered phase, the ordered traveling band of particles is formed, while in the disordered phase the flock displays disordered motion without the formation of the ordered traveling band. Comparing the ordered isotropic case with the ordered anisotropic case, we observe that the traveling band formed in the ordered case with $\alpha = 1$ is denser and narrower, indicating that the transition from the ordered state to the disordered state becomes more abrupt. In contrast, the traveling band in the ordered case with $\alpha = -1$ is sparser and wider, suggesting that the transition is less abrupt. It has been demonstrated that multiple density bands can emerge in much larger system sizes in the SVM [46,47]. To further investigate the impact of anisotropic interactions on the formation of traveling bands, simulation results for larger systems are shown in Figs. 5(e) and 5(f) for the AVM with $\alpha = 1$ and $\alpha = -1$, respectively. These results confirm that anisotropic interactions significantly affect the formation of traveling bands.

Thus, the anisotropic response to neighbors considerably impacts the relationship between noise intensity and collective motion, which for finite system sizes will appear to be even more pronounced (i.e., from a discontinuous transition for frontal bias to a continuouslike transition for rearward bias). In summary, we find that neighbors in front of a focal particle contribute to increasing the magnitude of first-order phase transitions, while neighbors behind weaken the strength of first-order phase transitions. To further and better understand how anisotropic interactions impact collective motion, we analyze even more minimal anisotropic models, a front-semicircle Vicsek model and a back-semicircle Vicsek model, in which each focal particle pays equal attention to near neighbors only in front or back of it, as shown in Figs. 1(d) and 1(e), respectively.

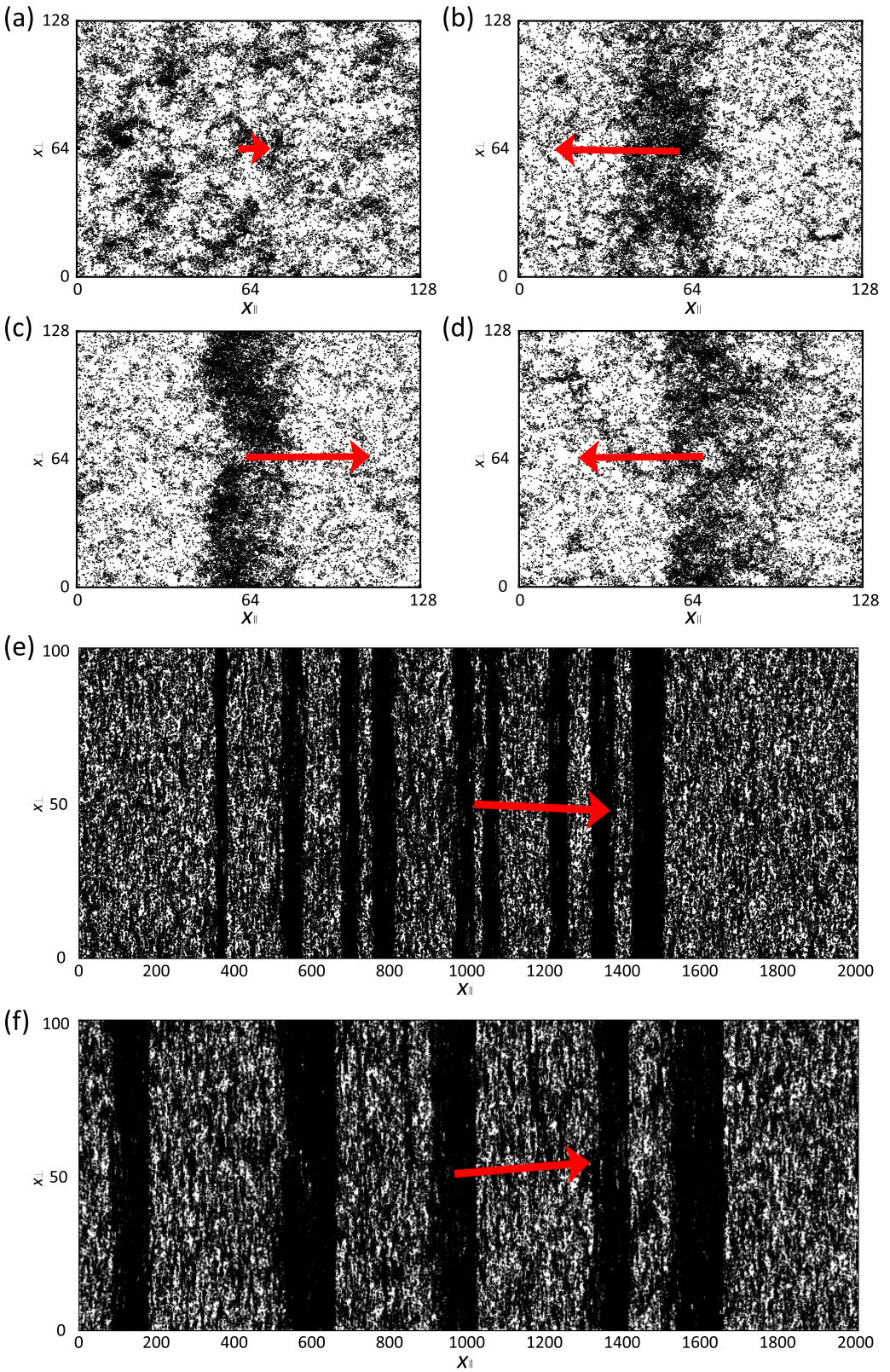

FIG. 5. Snapshots of the traveling flocks for the (a) disordered isotropic case with $\alpha = 0$, (b) ordered isotropic case with $\alpha = 0$, (c) ordered anisotropic case with $\alpha = 1$, and (d) ordered anisotropic case with $\alpha = -1$. $\varphi(t) \approx 0.09$ in the disordered case in (a), while $\varphi(t) \approx 0.36$ in the ordered cases in (b)–(d). Snapshots of the traveling flocks with multiple moving waves or bands in a rectangular domain of system size $L_\parallel \times L_\perp = 2000 \times 100$ with (e) $\alpha = 1$ and (f) $\alpha = -1$. Each red arrow indicates the traveling direction of motion of the flock. The length of the arrow indicates the speed (or magnitude) of the motion. The parameters are $\rho = 2$, $v_0 = 0.5$, and $L = 128$ for (a)–(d).

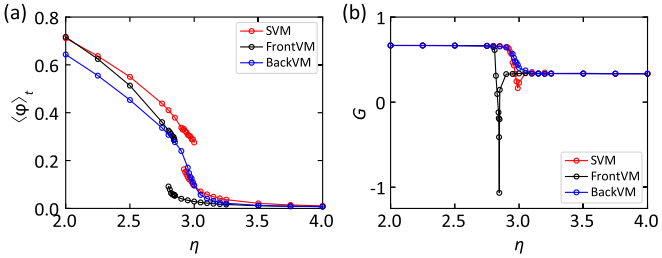

FIG. 6. Phase transitions of the front-semicircle Vicsek model and back-semicircle Vicsek model. (a) The time-averaged OP $\langle\varphi\rangle_t$ as a function of noise amplitude η. (b) Binder cumulant G as a function of noise amplitude η, with the same symbols and colors as in (a). Time averages are computed over 1×10^6 time steps. The parameters are $\rho = 2$, $v_0 = 0.5$, and $L = 128$.

Consistent with the above results, the FrontVM system exhibits a more pronounced first-order phase transition than the SVM, while the BackVM exhibits a weaker continuous-like phase transition, as shown in Fig. 6. Note that the nature of the phase transition in the BackVM is still first order in the thermodynamic limit (see the Appendix for a detailed analysis).

For further verification of the generality of the above findings, we additionally introduce the anisotropic social influence into the swarming model with vectorial noise proposed by Grégoire and Chaté [25]. As described above, angular noise can be considered action errors made by particles trying to take the new moving orientation that they perfectly calculated, while vectorial noise can be thought of as the errors made by individuals estimating the orientation or direction of others (thus, errors in each pairwise interaction, such as those due to sensory and/or environmental noise). The direction of travel (i.e., orientation) of each particle under vectorial noise conditions can be written as follows for the SVM and the AVM, respectively:

$$\langle\theta_i(t)\rangle_r = \Theta\left[\sum_{d_{ij}<r}^{n_i} \boldsymbol{v}_j(t) + \eta n_i \xi_i(t)\right], \tag{5}$$

$$\langle\theta_i(t)\rangle_r = \Theta\left[\boldsymbol{v}_i(t) + \sum_{d_{ij}<r, j\neq i}^{n_i-1} \Omega_{ij}\boldsymbol{v}_j(t) + \eta n_i \xi_i(t)\right]. \tag{6}$$

The impact of anisotropic influence on collective motion under the condition of vectorial noise is shown in Fig. 7. As reported in previous work [25,26], an already strong first-order phase transition is expected with isotropic influence for vectorial noise [red lines in Figs. 7(a)–7(c)]. For $\alpha > 0$, as α increases, the anisotropy first further enhances the gap in the order parameter $\langle\varphi\rangle_t$ at the transition between the ordered phase and the disordered phase, as we previously found with the model with angular noise (AVM). However, when $\alpha \gtrsim 1/4$, further increasing α shrinks the gap [Fig. 7(a)]. For $\alpha < 0$, as α decreases, anisotropy shrinks the gap monotonously [Fig. 7(b)]. As in FrontVM and BackVM, the gap between the ordered phase and disordered phase is enhanced by the frontal neighbors but shrunk by rearward neighbors [Fig. 7(c)]. Figure 7(d) shows the PDFs of $\varphi(t)$ near the transition point for BackVM.

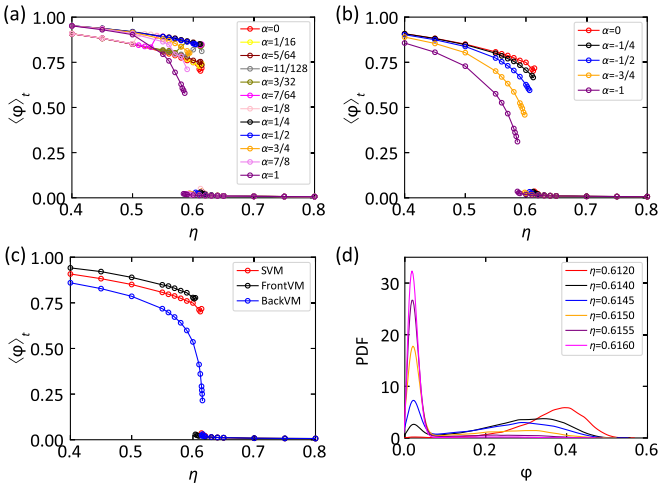

FIG. 7. Phase transitions of the swarming models with vectorial noise (a) and (b) for the AVM and (c) and (d) for the FrontVM and BackVM. (a) The time-averaged OP $\langle\varphi\rangle_t$ as a function of noise amplitude η for $\alpha \geqslant 0$. (b) $\langle\varphi\rangle_t$ versus the noise amplitude η for $\alpha \leqslant 0$. (c) $\langle\varphi\rangle_t$ versus the noise amplitude η for FrontVM and BackVM. The time-averaged OPs $\langle\varphi\rangle_t$ versus the noise amplitude η of the SVM are shown in red in (a)–(c). (d) Several probability density functions of $\varphi(t)$ near the transition point for BackVM. Time averages are computed over 1×10^6 time steps. The parameters are $\rho = 2$, $v_0 = 0.5$, and $L = 128$.

III. SUMMARY AND CONCLUSIONS

Here we analyzed the collective dynamics of a minimal model of self-propelled particles with anisotropic social interactions and investigated the impact of anisotropy on the collective motion exhibited as a function of different types (e.g., sources) of noise. We found that, if particles are influenced more strongly by neighbors in front than those behind, as the anisotropy becomes stronger, the system exhibits a monotonic progression from weak to stronger first-order phase transitions. By comparison, if each particle pays more attention to rearward neighbors, the system exhibits monotonic transitions from weak to weaker first-order phase transitions. Front-semicircle and back-semicircle Vicsek models, in which each particle pays equal attention only to the neighbors in front of it or in back of it, respectively, were also introduced to verify the robustness of these findings. In addition, these findings are robust to the nature of the noise (i.e., the same conclusions can be drawn for models with vectorial and scalar noise). Our results demonstrate that anisotropic interactions with neighbors based on their relative positions significantly impact the collective behavior of such systems. Frontal neighbors primarily enhance the strength of the first-order transition, whereas rearward neighbors progressively weaken it. The critical noise threshold required to achieve ordered motion decreases as α increases from zero to positive values. In contrast, while the threshold increases as α decreases from zero to negative values, the change is less pronounced. As system size (the number of particles) decreases, finite-size effects amplify the observed differences, resulting in what would appear to be a discontinuous first-order transition associated with frontal influence and a

continuouslike transition associated with rearward influence. Anisotropic response to neighbors may therefore be an important mechanism by which social transmission of information and thus collective motion, pattern formation, and decision-making in living systems may be tuned. Future research should further explore how anisotropic interactions influence collective behavior, as this factor could be crucial for understanding and modeling real-world collective motion, as well as for designing and controlling artificial systems like robotic swarms and autonomous vehicle networks.

ACKNOWLEDGMENTS

Z.G. gratefully acknowledges support from the China Scholarship Council (Grant No. 201806040105), the Max Planck Institute of Animal Behavior, the University of Konstanz, the School of Systems Science of the Beijing Normal University, and Prof. Zhangang Han. I.D.C. acknowledges support from the Deutsche Forschungsgemeinschaft (DFG, German Research Foundation) under Germany's Excellence Strategy—"Centre for the Advanced Study of Collective Behaviour" EXC 2117-422037984, the Max Planck Society, the European Union's Horizon 2020 research and innovation program under Marie Skłodowska-Curie Grant Agreement No. 860949, the DFG Gottfried Wilhelm Leibniz Prize 2022 584/22, the PathFinder European Innovation Council Work Programme 101098722, and Office of Naval Research Grant No. N0001419-1-2556.

APPENDIX: SWARMING TRANSITIONS OF SELF-PROPELLED PARTICLES WITH ANISOTROPIC SOCIAL INTERACTIONS

Order parameter time series near the transition point for the standard Vicsek model (top panel) and the anisotropic Vicsek model with $\alpha = 1$ (bottom panel) are shown in Fig. 8. It is clearly seen that the gap between the two phases (the ordered phase and the ordered phase) near the transition point of the anisotropic Vicsek model with $\alpha = 1$ is larger than that of

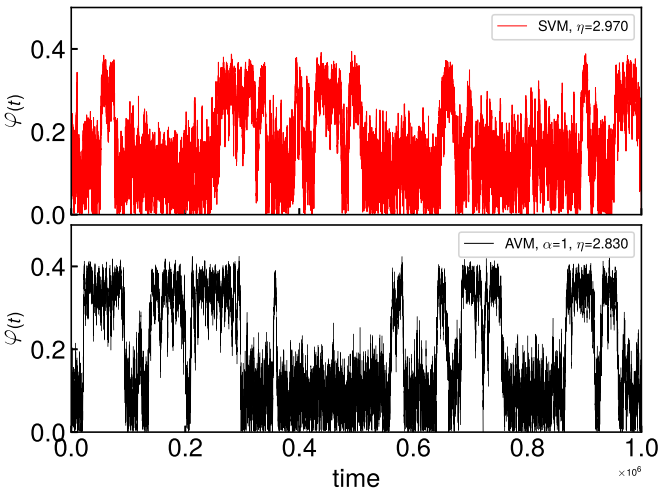

FIG. 8. Order parameter time series near the transition point of the standard Vicsek model (top panel) for $\eta = 2.970$ and the anisotropic Vicsek model with $\alpha = 1$ (bottom panel) for $\eta = 2.830$. The parameters are $\rho = 2$, $v_0 = 0.5$, and $L = 128$.

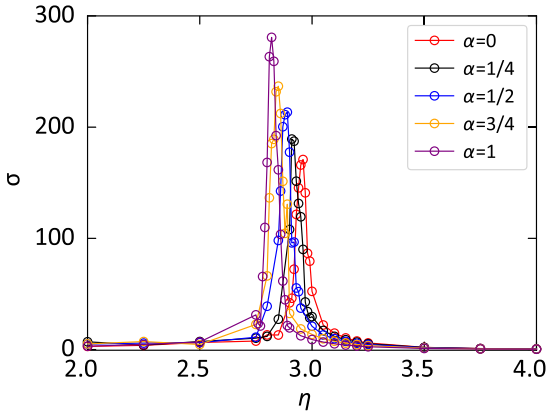

FIG. 9. Variance σ of $\varphi(t)$ in the anisotropic Vicsek model for $\alpha \geqslant 0$. The parameters are $\rho = 2$, $v_0 = 0.5$, and $L = 128$.

the standard Vicsek model, suggesting the first-order phase transition is enhanced and stronger in the anisotropic Vicsek model with $\alpha > 0$.

Studying the phase transition of biological systems of active entities or biologically inspired, inherently nonequilibrium models consisting of self-propelled particles is challenging [48]. Unlike equilibrium statistical mechanics, where the system can be described by well-established theories and phase transitions, nonequilibrium systems lack a universal framework. For example, there is no rigorous finite-size scaling theory for far-from-equilibrium phase transitions. However, researchers often apply knowledge and techniques derived from equilibrium systems to study these nonequilibrium systems. A common approach is finite-size scaling [5,26,49], which involves numerically estimating various moments of the order parameter distribution while systematically varying the system's linear size L. Particularly, the variance of the order parameter $\varphi(t)$, which represents the second moment, is considered a useful measure for quantifying and identifying phase transitions [26,49], as shown in the following equation, where L is the linear size of the system and d is the spatial dimension, with $d = 2$ in this case:

$$\sigma(\eta, L) = L^d\left(\langle\varphi^2\rangle_t - \langle\varphi\rangle_t^2\right). \tag{A1}$$

Studies of the regular Vicsek model, particularly for small to moderate system sizes, have shown that a peak occurs at the order-disorder state transition. This behavior suggests that the nonequilibrium system undergoes a continuous phase transition, as a large peak in the variance σ is typically considered a hallmark of a second-order phase transition in the theoretical framework of equilibrium systems. For example, Baglietto and Albano conducted an analysis of the Vicsek model at intermediate system sizes below a critical size L_c where high-density waves can emerge and found various critical exponents and hyperscaling relations that are characteristic of a second-order transition [49]. However, Chaté *et al.* showed that this critical size L_c appears to diverge as the density approaches both zero and infinity, resulting in a very unconventional "finite-size effect," where, for $L < L_c$, the system behaves as though it is undergoing a second-order transition [26]. If $L > L_c$, the transition exhibits a discontinuous nature, regardless of the form of the noise term. Therefore, a large peak in the variance σ, which appears to

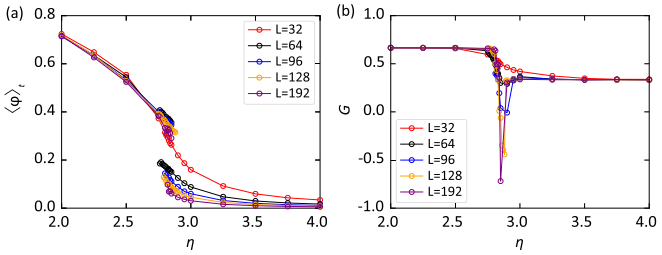

FIG. 10. Finite-size scaling analysis of the anisotropic Vicsek model with $\alpha = 1$. (a) Time-averaged order parameter and (b) Binder cumulant as a function of noise amplitude for various system sizes L. The parameters are $\rho = 2$ and $v_0 = 0.5$.

be a signature of a second-order phase transition, particularly for the Vicsek model, is actually caused by strong finite-size effects. As the system size L increases, the peak of σ gradually grows, eventually forming a Dirac δ-like peak (strong evidence of a first-order transition) for a sufficiently large L. This behavior is similar to what occurs with vectorial noise, where finite-size effects are less pronounced and a Dirac δ-like peak is easily observed at a small value of L [26]. Thus, the variance σ serves as a useful measure for quantifying phase transitions, and its peak position is often used to define the transition point, particularly in studies related to the Vicsek model.

As shown in Fig. 2 in the main text, for the anisotropic Vicsek model, the Binder cumulant G exhibits deeper minimum to negative values near the transition point as anisotropy α increases from 0 to 1, which indicates an enhanced discontinuous phase transition. As shown in Fig. 9, the variance σ becomes sharply peaked and increases in height, which can serve as evidence of a discontinuous phase transition, rather than being an artifact of a second-order phase transition caused by finite-size effects. Meanwhile, as shown in Figs. 2 and 4 in the main text, the transition point gradually decreases (i.e., shifts to the left) as α increases from 0 to 1. The peak position of the variance also shifts to the left, showing a consistent change trend. In fact, the peak position is often used to define the transition point.

Together with the time-averaged order parameter $\langle\varphi\rangle_t$ and the Binder cumulant G, σ provides consistent evidence of enhanced first-order phase transitions in the anisotropic Vicsek model as α increases from 0 to 1. All of these parameters can be used to quantify and identify the nature of phase transitions at small to moderate system sizes. Specifically, the gap in $\langle\varphi\rangle_t$, the minimum of the Binder cumulant G, and the trend of increasing or decreasing peak height of the variance σ can be used together to study phase transitions in Vicsek-like models, including the Vicsek model, at finite system size.

Finite-size scaling analysis of the anisotropic Vicsek model with $\alpha = 1$. Figure 10 shows the time-averaged order parameter [Fig. 10(a)] and Binder cumulant [Fig. 10(b)] as a function of noise amplitude for various system sizes L, along with probability density functions [Fig. 12(c)] of $\varphi(t)$ near the transition point. It is clearly seen that the Binder cumulant G exhibits a negative minimum and appears earlier near the transition point, indicating a stronger discontinuous nature of the phase transition when the system size is increased for the anisotropic Vicsek model with $\alpha = 1$ than for the standard Vicsek model. Thus, finite-size effects are weaker for the anisotropic Vicsek model with $\alpha > 0$.

Finite-size scaling analysis of the front-semicircle Vicsek model. Figure 11 shows the time-averaged order parameter [Fig. 11(a)] and Binder cumulant [Fig. 11(b)] as a function of noise amplitude for various system sizes L, along with probability density functions [Fig. 11(c)] of $\varphi(t)$ near the transition point. It is clearly seen that the Binder cumulant G exhibits a negative minimum and appears earlier near the transition point, indicating a stronger discontinuous nature of the phase transition when the system size is increased for the anisotropic Vicsek model than for the standard Vicsek model. Figure 11(c) shows more and more sharp bimodal peaks as the system size becomes larger, providing further evidence of the stronger discontinuous nature of the phase transition. Thus, finite-size effects are weaker for the anisotropic Vicsek model with $\alpha > 0$.

Finite-size scaling analysis of the back-semicircle Vicsek model. Figure 12 shows the time-averaged order parameter [Fig. 12(a)] and Binder cumulant [Fig. 12(b)] as a function of noise amplitude for various system sizes L, along with probability density functions [Fig. 12(c)] of $\varphi(t)$ near the transition point. It is clear that the Binder cumulant G exhibits a negative minimum when the system size is large enough, but the gap between the ordered phase and the disordered phase is much smaller than in both the front-semicircle Vicsek model and the standard Vicsek model. The nature of the phase transition for the back-semicircle Vicsek model is discontinuous but much weaker. Thus, finite-size effects are much stronger for the back-semicircle Vicsek model.

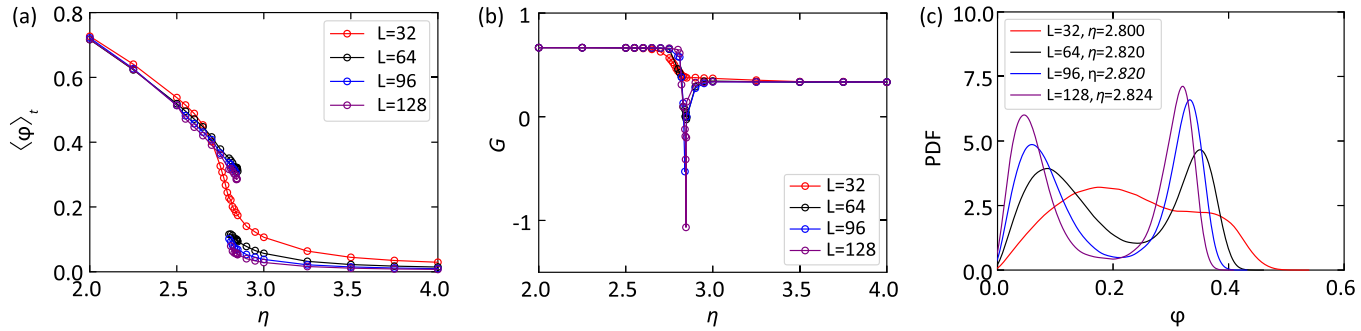

FIG. 11. Finite-size scaling analysis of the front-semicircle Vicsek model. (a) Time-averaged order parameter $\langle\varphi\rangle_t$ and (b) Binder cumulant G as a function of noise amplitude η for various system sizes L. (c) The probability density functions of $\varphi(t)$ near the transition point. The parameters are $\rho = 2$ and $v_0 = 0.5$.

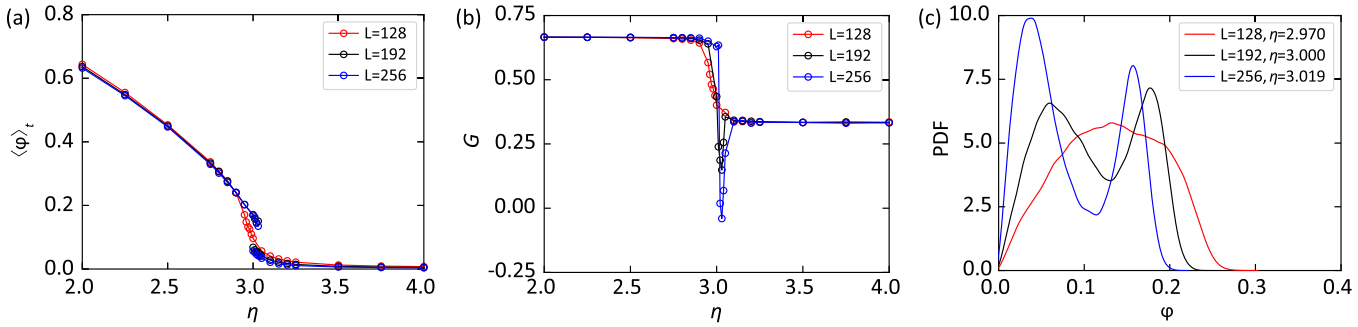

FIG. 12. Finite-size scaling analysis of the back-semicircle Vicsek model. (a) Time-averaged order parameter $\langle\varphi\rangle_t$ and (b) Binder cumulant G as a function of noise amplitude η for various system sizes L. (c) The probability density functions of $\varphi(t)$ near the transition point. The parameters are $\rho = 2$ and $v_0 = 0.5$.

[1] T. Vicsek and A. Zafeiris, Collective motion, Phys. Rep. **517**, 71 (2012).

[2] X. Chen, X. Dong, A. Be'er, H. L. Swinney, and H. P. Zhang, Scale-invariant correlations in dynamic bacterial clusters, Phys. Rev. Lett. **108**, 148101 (2012).

[3] G. De Palo, D. Yi, and R. G. Endres, A critical-like collective state leads to long-range cell communication in *Dictyostelium discoideum* aggregation, PLoS Biol. **15**, e1002602 (2017).

[4] C. Chen, S. Liu, X.-Q. Shi, H. Chaté, and Y. Wu, Weak synchronization and large-scale collective oscillation in dense bacterial suspensions, Nature (London) **542**, 210 (2017).

[5] A. Attanasi, A. Cavagna, L. Del Castello, I. Giardina, S. Melillo, L. Parisi, O. Pohl, B. Rossaro, E. Shen, E. Silvestri, and M. Viale, Finite-size scaling as a way to probe near-criticality in natural swarms, Phys. Rev. Lett. **113**, 238102 (2014).

[6] C. R. Reid, M. J. Lutz, S. Powell, A. B. Kao, I. D. Couzin, and S. Garnier, Army ants dynamically adjust living bridges in response to a cost–benefit trade-off, Proc. Natl. Acad. Sci. U.S.A. **112**, 15113 (2015).

[7] Y. Katz, K. Tunstrøm, C. C. Ioannou, C. Huepe, and I. D. Couzin, Inferring the structure and dynamics of interactions in schooling fish, Proc. Natl. Acad. Sci. USA **108**, 18720 (2011).

[8] J. E. Herbert-Read, A. Perna, R. P. Mann, T. M. Schaerf, D. J. T. Sumpter, and A. J. W. Ward, Inferring the rules of interaction of shoaling fish, Proc. Natl. Acad. Sci. USA **108**, 18726 (2011).

[9] J. Gautrais, F. Ginelli, R. Fournier, S. Blanco, M. Soria, H. Chaté, and G. Theraulaz, Deciphering interactions in moving animal groups, PLoS Comput. Biol. **8**, e1002678 (2012).

[10] K. Tunstrøm, Y. Katz, C. C. Ioannou, C. Huepe, M. J. Lutz, and I. D. Couzin, Collective states, multistability and transitional behavior in schooling fish, PLoS Comput. Biol. **9**, e1002915 (2013).

[11] M. Ballerini, N. Cabibbo, R. Candelier, A. Cavagna, E. Cisbani, I. Giardina, V. Lecomte, A. Orlandi, G. Parisi, A. Procaccini, M. Viale, and V. Zdravkovic, Interaction ruling animal collective behavior depends on topological rather than metric distance: Evidence from a field study, Proc. Natl. Acad. Sci. USA **105**, 1232 (2008).

[12] M. Nagy, Z. Ákos, D. Biro, and T. Vicsek, Hierarchical group dynamics in pigeon flocks, Nature (London) **464**, 890 (2010).

[13] A. Cavagna, A. Cimarelli, I. Giardina, G. Parisi, R. Santagati, F. Stefanini, and M. Viale, Scale-free correlations in starling flocks, Proc. Natl. Acad. Sci. USA **107**, 11865 (2010).

[14] D. J. Evangelista, D. D. Ray, S. K. Raja, and T. L. Hedrick, Three-dimensional trajectories and network analyses of group behaviour within chimney swift flocks during approaches to the roost, Proc. R. Soc. B **284**, 20162602 (2017).

[15] A. Flack, M. Nagy, W. Fiedler, I. D. Couzin, and M. Wikelski, From local collective behavior to global migratory patterns in white storks, Science **360**, 911 (2018).

[16] H. Ling, G. E. Mclvor, J. Westley, K. van der Vaart, R. T. Vaughan, A. Thornton, and N. T. Ouellette, Behavioural plasticity and the transition to order in jackdaw flocks, Nat. Commun. **10**, 5174 (2019).

[17] A. Strandburg-Peshkin, D. R. Farine, I. D. Couzin, and M. C. Crofoot, Shared decision-making drives collective movement in wild baboons, Science **348**, 1358 (2015).

[18] J. L. Silverberg, M. Bierbaum, J. P. Sethna, and I. Cohen, Collective motion of humans in mosh and circle pits at heavy metal concerts, Phys. Rev. Lett. **110**, 228701 (2013).

[19] A. Strandburg-Peshkin, C. R. Twomey, N. W. Bode, A. B. Kao, Y. Katz, C. C. Ioannou, S. B. Rosenthal, C. J. Torney, H. S. Wu, S. A. Levin, and I. D. Couzin, Visual sensory networks and effective information transfer in animal groups, Curr. Biol. **23**, R709 (2013).

[20] D. J. G. Pearce, A. M. Miller, G. Rowlands, and M. S. Turner, Role of projection in the control of bird flocks, Proc. Natl. Acad. Sci. USA **111**, 10422 (2014).

[21] I. D. Couzin, J. Krause, R. James, G. D. Ruxton, and N. R. Franks, Collective memory and spatial sorting in animal groups, J. Theor. Biol. **218**, 1 (2002).

[22] D. S. Calovi, U. Lopez, S. Ngo, C. Sire, H. Chaté, and G. Theraulaz, Swarming, schooling, milling: phase diagram of a data-driven fish school model, New J. Phys. **16**, 015026 (2014).

[23] T. Vicsek, A. Czirók, E. Ben-Jacob, I. Cohen, and O. Shochet, Novel type of phase transition in a system of self-driven particles, Phys. Rev. Lett. **75**, 1226 (1995).

[24] J. Toner and Y. Tu, Long-range order in a two-dimensional dynamical XY model: How birds fly together, Phys. Rev. Lett. **75**, 4326 (1995).

[25] G. Grégoire and H. Chaté, Onset of collective and cohesive motion, Phys. Rev. Lett. **92**, 025702 (2004).

[26] H. Chaté, F. Ginelli, G. Grégoire, and F. Raynaud, Collective motion of self-propelled particles interacting without cohesion, Phys. Rev. E **77**, 046113 (2008).
[27] E. Bertin, M. Droz, and G. Grégoire, Hydrodynamic equations for self-propelled particles: microscopic derivation and stability analysis, J. Phys. A **42**, 445001 (2009).
[28] T. Ihle, Invasion-wave-induced first-order phase transition in systems of active particles, Phys. Rev. E **88**, 040303(R) (2013).
[29] A. P. Solon and J. Tailleur, Revisiting the flocking transition using active spins, Phys. Rev. Lett. **111**, 078101 (2013).
[30] A. P. Solon and J. Tailleur, Flocking with discrete symmetry: The two-dimensional active Ising model, Phys. Rev. E **92**, 042119 (2015).
[31] R. Kürsten and T. Ihle, Dry active matter exhibits a self-organized cross sea phase, Phys. Rev. Lett. **125**, 188003 (2020).
[32] L. Jiang, L. Giuggioli, A. Perna, R. Escobedo, V. Lecheval, C. Sire, Z. Han, and G. Theraulaz, Identifying influential neighbors in animal flocking, PLoS Comput. Biol. **13**, e1005822 (2017).
[33] R. C. Hinz and G. G. de Polavieja, Ontogeny of collective behavior reveals a simple attraction rule, Proc. Natl. Acad. Sci. USA **114**, 2295 (2017).
[34] I. D. Couzin, J. Krause, N. R. Franks, and S. A. Levin, Effective leadership and decision-making in animal groups on the move, Nature (London) **433**, 513 (2005).
[35] I. D. Couzin, C. C. Ioannou, G. Demirel, T. Gross, C. J. Torney, A. Hartnett, L. Conradt, S. A. Levin, and N. E. Leonard, Uninformed individuals promote democratic consensus in animal groups, Science **334**, 1578 (2011).
[36] S. J. Simpson, G. A. Sword, P. D. Lorch, and I. D. Couzin, Cannibal crickets on a forced march for protein and salt, Proc. Natl. Acad. Sci. USA **103**, 4152 (2006).
[37] S. Bazazi, J. Buhl, J. J. Hale, M. L. Anstey, G. A. Sword, S. J. Simpson, and I. D. Couzin, Collective motion and cannibalism in locust migratory bands, Curr. Biol. **18**, 735 (2008).
[38] S. Bazazi, P. Romanczuk, S. Thomas, L. Schimansky-Geier, J. J. Hale, G. A. Miller, G. A. Sword, S. J. Simpson, and I. D. Couzin, Nutritional state and collective motion: from individuals to mass migration, Proc. R. Soc. B **278**, 356 (2011).
[39] V. Guttal, P. Romanczuk, S. J. Simpson, G. A. Sword, and I. D. Couzin, Cannibalism can drive the evolution of behavioural phase polyphenism in locusts, Ecol. Lett. **15**, 1158 (2012).
[40] R. S. Negi, R. G. Winkler, and G. Gompper, Emergent collective behavior of active Brownian particles with visual perception, Soft Matter **18**, 6167 (2022).
[41] R. S. Negi, R. G. Winkler, and G. Gompper, Collective behavior of self-steering active particles with velocity alignment and visual perception, Phys. Rev. Res. **6**, 013118 (2024).
[42] P. Romanczuk, I. D. Couzin, and L. Schimansky-Geier, Collective motion due to individual escape and pursuit response, Phys. Rev. Lett. **102**, 010602 (2009).
[43] A. Filella, F. Nadal, C. Sire, E. Kanso, and C. Eloy, Model of collective fish behavior with hydrodynamic interactions, Phys. Rev. Lett. **120**, 198101 (2018).
[44] T. Xue, X. Li, P. Grassberger, and L. Chen, Swarming transitions in hierarchical societies, Phys. Rev. Res. **2**, 042017(R) (2020).
[45] K. Binder, Applications of Monte Carlo methods to statistical physics, Rep. Prog. Phys. **60**, 487 (1997).
[46] H. Chaté, F. Ginelli, G. Grégoire, F. Peruani, and F. Raynaud, Modeling collective motion: variations on the Vicsek model, Eur. Phys. J. B **64**, 451 (2008).
[47] H. Chaté, Dry aligning dilute active matter, Annu. Rev. Condens. Matter Phys. **11**, 189 (2020).
[48] E. F. W. Heffern, H. Huelskamp, S. Bahar, and R. F. Inglis, Phase transitions in biology: from bird flocks to population dynamics, Proc. R. Soc. B **288**, 20211111 (2021).
[49] G. Baglietto and E. V. Albano, Finite-size scaling analysis and dynamic study of the critical behavior of a model for the collective displacement of self-driven individuals, Phys. Rev. E **78**, 021125 (2008).